ELSEVIER

Polymer 43 (2002) 1667–1679

polymer

www.elsevier.com/locate/polymer

Superheating of the melting kinetics in polymer crystals: a possible nucleation mechanism

Akihiko Toda[a,*], Masamichi Hikosaka[a], Koji Yamada[b]

[a]*Faculty of Integrated Arts and Sciences, Hiroshima University, 1-7-1 Kagamiyama, Higashi-Hiroshima 739-8521, Japan*
[b]*Oita Research Center, Sun Allomer Ltd., 2 Oaza-Nakanosu, Oita 870-0189, Japan*

Received 27 August 2001; received in revised form 1 November 2001; accepted 2 November 2001

Abstract

Melting kinetics of polymer crystals has been examined experimentally by calorimetric methods utilizing the combination of a conventional differential scanning calorimetry of heat flux type (CDSC-HF) and a temperature-modulated DSC (TMDSC). The superheating effect in the kinetics has been discussed based on a modeling of the melting kinetics. For low-density polyethylene and linear polyethylene, the melting rate showed nearly linear dependence on the degree of superheating, which indicates the kinetics controlled by heat diffusion or by surface kinetics on rough interface. For isotactic polypropylene, poly(ethylene terephthalate) and poly(ϵ-caprolactone), the dependence is non-linear and close to the limiting case of exponential dependence, which indicates nucleation-controlled kinetics of melting. A possible mechanism of the activation process in the melting kinetics has been discussed in consideration of the specific feature of polymer crystals far from its most stable state. The consistency of the results of CDSC-HF and TMDSC has been confirmed by this analysis with a calibration of peak temperature for the instrumental thermal delay in CDSC-HF.

Keywords: Melting; Differential scanning calorimetry; Calibration

1. Introduction

Endothermic peak in the melting region of polymer crystals shows a complicated behavior in its heating rate dependence [1]. For slow heating rate, the peak temperature increases with lowering heating rate, but for faster heating rate, it increases with increasing the rate. In this behavior, the dependence with slow heating rate is supposed to be caused by recrystallization and/or reorganization which shift melting point to higher temperature. Recrystallization and reorganization are slow processes compared with melting, and hence those processes are more effective with slow heating rate. Therefore, crystals become more perfect (and thicker) and increase melting peak temperature with slower heating rate. On the other hand, for faster heating rate, those processes are not well advanced before crystals melt, and hence the increase in melting temperature is less pronounced. Under the condition, if the melting is not instantaneous, the peak temperature will shift to higher temperature with faster heating rate. This behavior is called superheating because the crystals are in a temperature above the melting point. For example [1–4], with extended chain crystals, recrystallization or reorganization does not occur and the melting peak temperature shows a significant increase with faster heating rate. In the present paper, we discuss the superheating effect observed with a conventional differential scanning calorimetry (CDSC), based on a modeling of the melting kinetics to clarify the characteristic mechanism in polymer crystals. The results of CDSC are also examined in terms of its consistency with the results of 'periodically modulated driving force' [5–17] applied by a temperature modulated DSC (TMDSC) [18–23]. On the basis of those results, we discuss the possibility of nucleation-controlled process of melting in polymer crystals.

TMDSC applies a periodic modulation in temperature to a linear heating (or cooling) and examines the response in heat flow to determine the heat capacity from the modulation components of temperature and heat flow [18–23]. In the melting region, the melting kinetics responds to the modulation in temperature, and hence the heat capacity becomes an apparent one including the response of latent heat. When the transition temperature distributes over a broad temperature range, as in the case of the melting region of polymer crystals, with the periodic modulation to the linear heating we can attain a steady response of the system as a total sum of the response of the melting kinetics of each crystallite. Therefore, the melting kinetics can be analyzed

* Corresponding author. Tel.: +81-824-24-6558; fax: +81-824-24-0757.
E-mail address: atoda@hiroshima-u.ac.jp (A. Toda).

0032-3861/02/$ - see front matter
PII: S0032-3861(01)00733-9

with the Fourier analysis of the response, which is applied to determine the heat capacity from the modulation components. By examining with different modulation frequency covering the characteristic time, τ_{TM}, of melting of each crystallite, the apparent heat capacity shows a frequency dispersion, from which we can determine τ_{TM} [10–15].

The characteristic time, τ_{TM}, characterizes the quickness of melting transition of each crystallite. The rate of first-order transition, in general, is a function of the distance from transition temperature, ΔT, namely the degree of superheating in the case of melting. With faster heating rate β, ΔT becomes higher in a shorter time interval, and hence the characteristic time of melting, τ_{TM}, becomes shorter. The dependence of τ_{TM} on the underlying heating rate, β, is therefore determined by the dependence on ΔT of melting rate, and hence ΔT dependence of melting rate can be evaluated from the β dependence of τ_{TM}. We have applied this analysis of periodically modulated driving force to the kinetics of crystallization [5–9], melting [10–15], solid-state transition [16], and chemical reaction [17] of polymeric systems. We have successfully shown that the ΔT dependence of transition rate or the activation energy of chemical reaction is obtainable by this method. The characteristic time, τ_{TM}, in the melting region must be related with the superheating observed by CDSC, and an approach based on this expectation has been made by Schawe and Strobl [24]. In the present paper, we discuss the relationship in a quantitative manner.

It is known that a pure metal standard such as indium, which is supposed to melt at a single transition point with negligibly small superheating, also exhibit the increase in peak temperature and onset temperature with faster heating rate. This behavior must be an apparent shift due to instrumental delay determined by the thermal contact between sample pan and the monitoring station of sample temperature. Therefore, it is required to evaluate the apparent shift to discuss the true shift caused by superheating in the melting region of polymer crystals. There has been an empirical method of temperature calibration using the onset temperature of melting of standard materials at the respective heating rates [25]. However, the apparent shift due to instrumental effect of the peak temperature in the melting of polymer crystals depends on the peak height and the slope [26], and hence the shift cannot be fully calibrated by this method. Danley and Caulfield of TA Instruments [27] recently proposed a method to construct the heat flow and sample temperature from the temperature data at the monitoring station and at the heat source with the instrumental coefficients pre-determined by a standard sample. With this method, true heat flow from the sample can be plotted against true sample temperature, and hence the instrumental thermal delay is automatically calibrated by this procedure. In the following, we apply this procedure to examine the heating rate dependence of melting peak temperature of polymer crystals.

To see the superheating effect in the melting of polymer crystals, it is also necessary to avoid recrystallization and reorganization. In order to do this in the present analysis, samples are annealed near the melting temperature to increase the perfection (and thickness) of crystals and minimize the change in melting point on subsequent heating run.

In the following, we firstly discuss the apparent shift caused by the instrumental delay, based on the Mraw's model [28] of DSC of heat flux type (CDSC-HF). Then, we discuss the heating rate dependence of the melting peak with a modeling of the melting kinetics and examine the relationship between the degree of superheating determined by CDSC-HF and the characteristic time obtained by TMDSC. The analysis is examined experimentally with isotactic polypropylene (iPP), low-density polyethylene (LDPE), linear polyethylene (PE), poly(ethylene terephthalate) (PET), and poly(ϵ-caprolactone) (PCL), showing different ΔT dependences of melting rate.

2. Modeling

2.1. Modeling of CDSC-HF

In a conventional DSC of heat flux type (CDSC-HF), the temperature at a heat source is controlled and the sample temperature is detected at the monitoring station which has a close contact with the sample. Following the Mraw's model [28], DSC of heat flux type is modeled by heat transfer coefficients and the heat capacities of those parts shown in Fig. 1. The equations describing the heat flow in terms of sample side are expressed as follows:

$$C_s \frac{dT_s}{dt} = K_1(T_m - T_s) + F \tag{1}$$

$$C_m \frac{dT_m}{dt} = K_1(T_s - T_m) + K_0(T_h - T_m) \tag{2}$$

$$T_h = T_{0h} + \beta t \tag{3}$$

where T_s, T_m, and T_h represent sample temperature, temperature of monitoring station, and temperature of heat source, respectively, and C_s and C_m are the heat capacity of sample + sample pan and the heat capacity of monitoring station, respectively. The temperature of heat source is

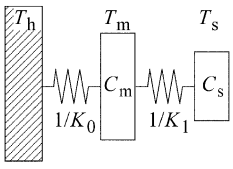

Fig. 1. Schematic representation of the Mraw's model describing a DSC of heat flux type for the sample side; T_h, T_m and T_s represent the temperatures of the heat source, monitoring station and sample, respectively. The Newton's law constants of heat transfer between the heat source and the monitoring station and between the monitoring station and the sample are K_0 and K_1, respectively. The heat capacities of the monitoring station and sample + sample pan are represented as C_m and C_s, respectively.

controlled to be heated up at the constant rate, β. The heat transfer coefficients between heat source and monitoring station and between monitoring station and sample are represented as K_0 and K_1, respectively. Finally, absorbed or released heat flow on transformation is represented by F with negative sign for endothermic process.

The calibration method proposed by Danley and Caulfield [27] is based on the Mraw's model. By determining the instrumental coefficients with a standard sample, the sample temperature, T_s, and heat flow, F, is calculated from the obtainable data of the temperature at the monitoring station, T_m, and that of heat source, T_h, with Eqs. (1)–(3). The method described below is essentially the same as the one proposed by Danley and Caulfield. The difference is on the details of the determination method of the instrumental coefficients and on the determination of T_h utilizing T_m in the present method.

When applied to the melting of a pure metal such as indium with negligible superheating and negligible change in C_s on melting, the solutions are obtained for three separate stages before melting ($t < t_{start}$), during melting ($t_{start} < t < t_{end}$), and after melting ($t_{end} < t$) [29]. Before melting the sample temperature undergoes linear heating, during melting the temperature of sample pan is kept at the melting point, and after melting the temperature returns to linear heating with a relaxation time due to instrumental time constants (Fig. 2a and b);

for $t < t_{start}$,

$$T_{s1} = T_{0b} + \beta t - \beta\left(\frac{C_s}{K_1} + \frac{C_s + C_m}{K_0}\right) \tag{4}$$

$$T_{m1} = T_{0b} + \beta t - \beta\frac{C_s + C_m}{K_0} \tag{5}$$

for $t_{start} < t < t_{end}$,

$$T_{s2} = T_M = T_{0b} + \beta t_{start} - \beta\left(\frac{C_s}{K_1} + \frac{C_s + C_m}{K_0}\right) \tag{6}$$

$$T_{m2} = T_M + \beta\frac{C_s}{K_1} + \alpha\Delta t_2 + \frac{K_1}{(K_0 + K_1)^2}\beta C_m\left(1 - e^{-\frac{K_0+K_1}{C_m}\Delta t_2}\right) \tag{7}$$

$$\Delta t_2 \equiv t - t_{start} \tag{8}$$

$$\alpha \equiv \frac{K_0}{(K_0 + K_1)}\beta \tag{9}$$

where T_M represents the melting point,

and for $t_{end} < t$,

$$T_{s3} = T_{0b} + \beta t - \beta\left(\frac{C_s}{K_1} + \frac{C_s + C_m}{K_0}\right) + a_1 e^{-\lambda_1\Delta t_3} + a_2 e^{-\lambda_2\Delta t_3} \tag{10}$$

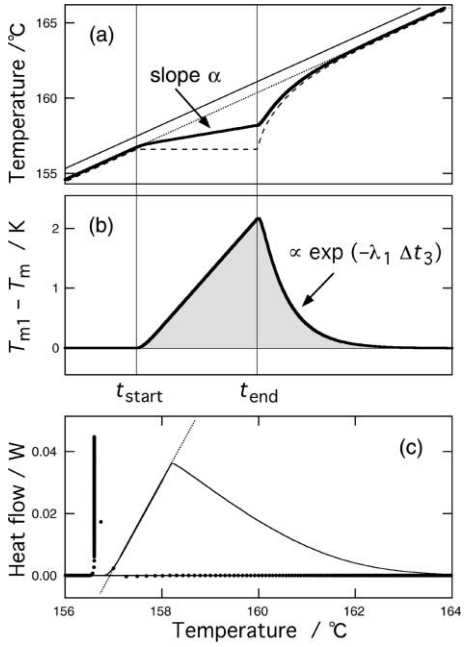

Fig. 2. A numerical calculation of Eqs. (1)–(3) to simulate the melting of indium: (a) T_h (thin line), T_m (thick line), T_s (broken line) and T_{m1} (dotted line), and (b) $T_{m1} - T_m$. In (c), the heat flow on transition, F, (●) was reconstructed from T_m, T_h, and T_s with Eq. (1) and plotted against T_s. The full line in (c) represents K_0 ($T_{m1} - T_m$) plotted against T_m, which corresponds to the output heat flow signal of CDSC on transition. In (c), the intersection point of dotted line with zero line defines the onset temperature, T_m^{onset}, of Eq. (15). For the kinetics, a melting rate coefficient of R with $a = 10^6 \gg 1$ and $y = 1$ in Eq. (16) was assumed for the single melting point. Heating rate was 10 K min^{-1} and the coefficients in Eqs. (1)–(3) were $C_s = 25$ mJ K^{-1}, $C_m = 40$ mJ K^{-1}, $K_0 = 13.7$ mW K^{-1} and $K_1 = 24$ mW K^{-1}, assuming nitrogen purge gas. Sampling interval was 0.2 s.

$$T_{m3} = T_{0b} + \beta t - \beta\frac{C_s + C_m}{K_0} + b_1 e^{-\lambda_1\Delta t_3} + b_2 e^{-\lambda_2\Delta t_3} \tag{11}$$

$$\Delta t_3 \equiv t - t_{end} \tag{12}$$

where λ_1 and λ_2 are the solutions of the following equation ($0 < \lambda_1 < \lambda_2$),

$$\lambda^2 - \left(\frac{K_1}{C_s} + \frac{K_1}{C_m} + \frac{K_0}{C_m}\right)\lambda + \frac{K_0 K_1}{C_s C_m} = 0 \tag{13}$$

and a_1, a_2, b_1 and b_2 are constants determined by the continuation of T_s and T_m.

The instrumental effects appear in the heating rate of monitoring station, α, during melting (Fig. 2a), the relaxation time, $\tau_{re} \equiv 1/\lambda_1$, which characterizes the recovering process of temperature to linear heating after the melting (Fig. 2b), the integration of the deviation of T_m from linear increase, which corresponds to the change in total enthalpy on melting (Fig. 2b), and the heating rate dependence of 'onset' temperature of melting, T_m^{onset}, defined by the intersection of the extrapolation of the linear increase in heat flow on transition (Fig. 2c). The integrated heat flow is

represented as,

$$K_0\left\{\int_{t_{start}}^{t_{end}}(T_{m2}-T_{m1})dt+\int_{t_{end}}^{\infty}(T_{m3}-T_{m1})dt\right\}=\Delta H_f \quad (14)$$

where ΔH_f represents the total change in enthalpy. The heating rate dependence of onset temperature is expressed as,

$$T_m^{onset}=T_M+\beta\left(\frac{C_s}{K_1}+\frac{C_m}{K_0+K_1}\right) \quad (15)$$

Utilizing the expressions of Eqs. (9), (13)–(15), the instrumental coefficients, C_m, K_0 and K_1, can be determined experimentally.

With the instrumental coefficients and the heat capacity of sample + sample pan, C_s, pre-determined by TMDSC with a standard method, it is possible to deconvolute the instrumental effect by calculating the sample temperature, T_s, and the heat flow on transition, F, from the experimental data of temperature at the monitoring station of sample side, T_m, following Eqs. (1)–(3), as follows. Firstly, if the temperature data of heat source, T_h, is not available as in the case of DSC 2920 (TA Instruments) used in the present experiments, T_h, of Eq. (3) can be reconstructed from the data of T_{m1} with Eq. (5) for the stage of $t < t_{start}$. Then, T_s is determined from T_m and T_h with Eq. (2), and F from T_m, T_h and T_s with Eq. (1). Fig. 2c shows an example for the sharp transition, which should have a single peak at the transition point when plotted against sample temperature, T_s.

2.2. Modeling of melting kinetics of polymer crystallites

2.2.1. CDSC-HF

We model the melting kinetics of polymer crystallites by the simplest kinetic equation of the change in crystallinity, ϕ, with a rate coefficient, R, dependent on superheating, ΔT, as follows,

$$\frac{d\phi(t)}{dt}=-R(\Delta T)\phi(t) \quad (16)$$

$$R(\Delta T)\equiv a\Delta T^y \quad (17)$$

where a and y are constants. The equation is easily integrated under the condition of linear heating with the rate of β, as follows,

$$\phi(\Delta t>0)=\phi_0(T_M)\exp\left[-\left(\frac{\Delta t}{\tau_c}\right)^{y+1}\right] \quad (18)$$

$$\tau_c\equiv(y+1)^{\frac{1}{y+1}}a^{-\frac{1}{y+1}}\beta^{-x} \quad (19)$$

$$x=\frac{y}{y+1} \quad (20)$$

where $\Delta t\equiv t-t_0$ with $T_s=T_M$ at $t=t_0$ and $\phi_0(T_M)$ represents the distribution function of melting points, T_M. Here, τ_c defines the mean time of melting of each crystallite on heating and the heating rate dependence of $\tau_c(\beta)$ expressed by the power, $-x$, is determined by the power, y, of the ΔT dependence of melting rate coefficient expressed as Eq. (17).

The endothermic heat flow on melting, F, is in proportion to the change in total crystallinity, Φ, which is given by the convolution of the kinetics with the distribution function of melting points, as follows:

$$\Phi(t)=\int_0^{\infty}dT_M\phi_0(T_M)\exp\left[-\left(\frac{\Delta t}{\tau_c}\right)^{y+1}\right] \quad (21)$$

$$F(t)=\Delta H_f\frac{d}{dt}\Phi(t) \quad (22)$$

The characteristic time, τ_c, can be determined from the shift in peak temperature, ΔT_{shift}, due to superheating effect with different heating rate, β. From the results of a numerical calculation shown in Fig. 3, it is seen that the following relationship among them is approximately satisfied

$$\Delta T_{shift}\equiv T_s^{peak}(\beta)-T_s^{peak}(0)\cong\beta\tau_c\propto\beta^z \quad (23)$$

$$z=1-x \quad (24)$$

The correction factor, $\Delta T_{shift}/\beta\tau_c$, is shown in Fig. 3b; the relationship strictly holds for the limiting case of $z\to 0$ ($y\to\infty$) because $\phi(\Delta t)$ becomes a step function with a sudden change at $\Delta t=\tau_c$.

Before applying this relationship in order to analyze the peak temperature obtained by CDSC-HF, we need to deconvolute the instrumental effect described by Eqs. (1)–(3) with the instrumental coefficients determined by the melting of indium.

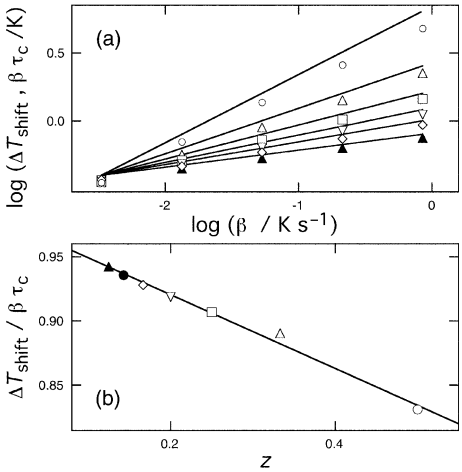

Fig. 3. A numerical calculation of Eqs. (21) and (22) for the relationship among the shifts in peak temperature, ΔT_{shift}, the characteristic time, τ_c, and heating rate, β. The symbols represent the results for $y=1$ (○), 2 (△), 3 (□), 4 (▽), 5 (◇), 6 (●), and 7 (▲). The straight lines in (a) represent $\beta\tau_c$ calculated from Eq. (19) for the respective values of y. In (b), the correction factor, $\Delta T_{shift}/\beta\tau_c$, for the expression of Eq. (23) is plotted against z. Heating rate was taken as 0.2, 0.8, 3.2, 12.8, and 51.2 K min^{-1} and the coefficient, a, in τ_c of Eq. (19) was chosen to set $\tau_c=120$ s at $\beta=0.2$ K min^{-1}.

2.2.2. TMDSC [10,11,13]

In the method of periodically modulated driving force, we apply a periodic modulation in sample temperature in addition to linear heating in order to see the frequency dispersion determined by the response of melting kinetics to the modulation in superheating. The frequency dispersion appears in the apparent heat capacity determined from the modulation components of temperature and heat flow obtained by TMDSC. Applying an appropriate calibration of the instrumental effects [14], the true response of the transformation kinetics can be determined. It has been confirmed that the frequency dependence can be roughly approximated as a frequency response function of Debye's type, as follows,

$$\widetilde{\Delta C}\,\mathrm{e}^{-\mathrm{i}\alpha} \equiv \widetilde{\Delta C}' - \mathrm{i}\widetilde{\Delta C}'' \cong C_\mathrm{s} + \frac{|\bar{F}/\beta|}{1 + \mathrm{i}\omega\tau_\mathrm{TM}(\beta)} \tag{25}$$

where $\bar{F}$ represents the mean endothermic heat flow on melting, which is obtained from 'total' heat flow, which is determined by averaging modulated heat flow over one period. With the expression of Eq. (25), the response of the kinetics for the limiting case of instantaneous transition ($\omega\tau_\mathrm{TM} \ll 1$) appears in the real part of the apparent heat capacity because the transition follows the change in temperature without delay and the heat flow is indistinguishable from the heat flow with true heat capacity. On the other hand, for the limiting case of slow transition ($\omega\tau_\mathrm{TM} \gg 1$) the response is controlled by the transition rate which is a function of ΔT and out of phase from the time derivative of modulated temperature, and hence the response appears in the imaginary part of the apparent heat capacity.

The time constant, τ_TM, as well as τ_c characterizes the quickness of the kinetics; τ_c represents the mean residence time in the state of superheating and determines the degree of ΔT_shift related to the position of the peak in $\dot{\phi}$, while τ_TM corresponds to the width of the peak, namely the mean time required from the onset of transition until its completion, and determines the modulation in heat flow, which is in proportion to $\dot{\phi}$. The difference between them becomes larger for stronger dependence of R on ΔT (larger y), as shown below, because of longer induction time (longer τ_c) and sudden increase in R (shorter τ_TM) for the stronger dependence. The dependence on underlying heating rate, β, of τ_TM is the consequence of earlier completion of melting with faster heating rate because of faster increase in superheating. Therefore, the dependence is determined by the superheating dependence of the melting rate coefficient, $R(\Delta T)$. Numerical calculation for different types of ΔT dependences of R given by Eq. (17) suggests that the following relationship holds between τ_c and τ_TM,

$$\frac{\tau_\mathrm{c}}{\tau_\mathrm{TM}} = (y + 1) \tag{26}$$

This result means that the characteristic time, τ_TM, obtained by TMDSC has the following expression,

$$\tau_\mathrm{TM} = (y + 1)^{-\frac{y}{y+1}} a^{-\frac{1}{y+1}} \beta^{-x} \tag{27}$$

The characteristic time, τ_TM, can be determined from the frequency dependence of the apparent heat capacity based on the expression of Eq. (25). Figs. 4 and 5 shows a typical example of the frequency dispersion in the melting region of polymer crystals. From the peak frequency seen in Fig. 5b, the characteristic time is determined as $\tau_\mathrm{TM} = 1/\omega_\mathrm{peak}$, The characteristic time can also be determined from the asymptotic behavior of Eq. (25) expressed as follows for

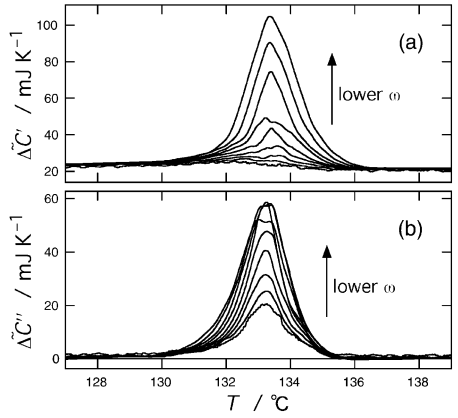

Fig. 4. Apparent heat capacity obtained by TMDSC in the melting region of PE. The underlying heating rate was 0.8 K min^{-1} and the modulation period was 13, 17, 22, 28, 36, 47, 60, 78 and 100 s. Sample was 1.14 mg in weight and 44 μm in thickness.

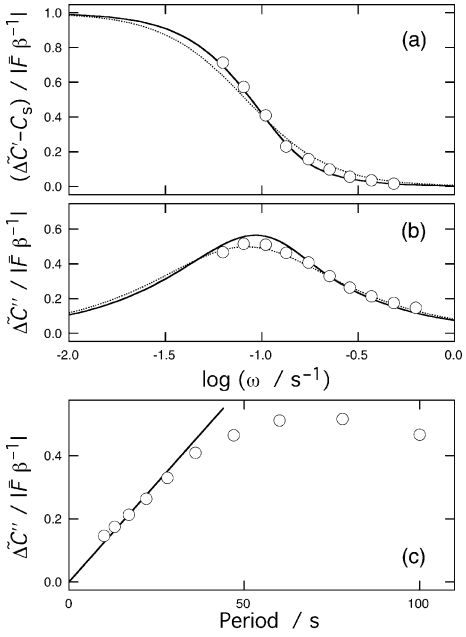

Fig. 5. Frequency dependence of the complex heat capacity shown in Fig. 4 at the peak temperature. The full lines in (a) and (b) represent analytical solution for the linear dependence on superheating of melting rate, $R \propto \Delta T$, and the dotted lines are for the exponential dependence, $\log R \propto \Delta T$, which corresponds to the limiting case of $y \to \infty$. The asymptotic behavior of Eq. (28) is shown in (c).

$\omega\tau_{TM} \gg 1$ (Fig. 5d),

$$\frac{\Delta C''}{|\bar{F}/\beta|} \cong \frac{1}{\omega\tau_{TM}} \tag{28}$$

3. Experimental

A DSC 2920 Module controlled with Thermal Analyst 2200 (TA Instruments) was used for all measurements. Helium or nitrogen gas with a flow rate of 40 ml min^{-1} was purged through the cell. Reference pan was removed in all experiments [30].

The polymer samples were thin films, the thickness of which was less than 100 μm in most cases. The characteristics of samples are the following: isotactic polypropylene (iPP, Sun Allomer Ltd, $M_w = 9.0 \times 10^4$ and the isotactic pentad fraction of [mmmm] = 99.2%), low-density polyethylene (LDPE, NIST SRM1473), linear polyethylene (PE, NIST SRM1475, $M_w = 5.2 \times 10^4$ and $M_w/M_n = 2.9$), poly(ethylene terephthalate) (PET, Toyobo Co., Ltd., $M_w = 2.5 \times 10^4$), and poly(ϵ-caprolactone) (PCL, Scientific Polymer Products, Inc., $M_w = 3.0 \times 10^4$). Samples were cut into the shape of a disk to fit the interior of sample pan in order to avoid the deformation of the aluminum pan on crimping, namely to minimize the change in the coefficient of the thermal contact between the bottom of sample pan and the monitoring station, K_1. The samples in an aluminum pan were melted, crystallized and annealed close to the melting temperature. The details of the conditions are the following; (1) iPP was melted at 200 °C, crystallized at 110 °C for 10 min, and annealed at 165 °C for 2 h, (2) LDPE was melted at 140 °C, crystallized by a rapid cooling of $\beta = 20$ K min^{-1} to 20 °C and annealed at 103 and 90 °C for 24 h each time, subsequently, (3) PE was melted at 150 °C, crystallized by a cooling of $\beta = 10$ K min^{-1} to 100 °C, and annealed at 130 °C for 3 h, (4) PET was melted at 280 °C, crystallized at 225 °C for 1 h, and annealed at 255 °C for 2 h, (5) PCL was melted at 120 °C, crystallized by a rapid cooling of $\beta = 20$ K min^{-1} to 20 °C, heated up to 57 °C, which was above one of the double melting peaks, and then annealed at 50 °C for 1 week. It has been confirmed that the annealing with longer interval than the above does not change the heating rate dependence of melting peak temperature even with the slowest heating rate, and hence recrystallization and reorganization will be negligible under the present conditions (>0.2 K min^{-1}).

With CDSC, the melting behaviors of those samples were examined at the heating rate of 0.2–40 K min^{-1} with the sampling interval of 0.2 s. With TMDSC, the rate of underlying heating rate was in the range of 0.2–1.6 K min^{-1}. Sinusoidal temperature modulation was applied with the modulation period in the range of 10–100 s and the amplitude satisfying 'heating only' condition, $dT_m/dt > 0$. For the correction of the magnitude of complex heat capacity obtained with TMDSC, the calibration coefficient has been adjusted for the data outside the transition region. Concerned with the phase angle, a baseline has been chosen to set the phase angle to zero degrees outside the transition region. This calibration is justified for relatively small peak of the apparent heat capacity, the condition of which is satisfied with the small mass of sample for the melting of polymer crystals. The difference of the results with this calibration and more accurate one [14] based on Hatta's method [30] was less than 10%. The condition of (quasi-) steady response of transition kinetics has been confirmed by plotting Lissajous diagram of the modulation components of heat flow and temperature for two or three cycles of the data having a closed loop.

4. Results

4.1. Melting of indium

Fig. 6 shows a typical temperature change at the monitoring station of sample side. Utilizing Eqs. (9), (13)–(15), the instrumental coefficients, C_m, K_0 and K_1, have been determined from the heating rate, α, during the melting, the relaxation time, τ_{re}, which has been determined from the plot shown in Fig. 6c, the integrated area of the peak in Fig. 6b, and the onset temperature, T_m^{onset}. In the calculation, we utilized the value of heat capacity of sample + sample pan, C_s, determined from TMDSC with a standard method. The instrumental coefficients optimizing the experimental results with $\beta = 0.2$, 2, 10, 20, 30 and 40 K min^{-1} are summarized as follows: $C_m = 40$ mJ K^{-1},

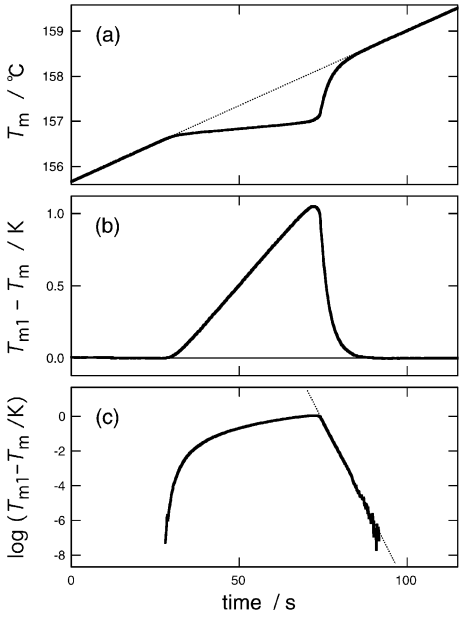

Fig. 6. Temperature change at the monitoring station of sample side, T_m, in the melting of indium on heating at $\beta = 2$ K min^{-1} under helium purge gas: (a) T_m (thick line) and T_{m1} (dotted line), (b) $T_{m1} - T_m$, and (c) log($T_{m1} - T_m$). In (c), the slope of the dotted line determines τ_{re}. The sample mass was 22.84 mg.

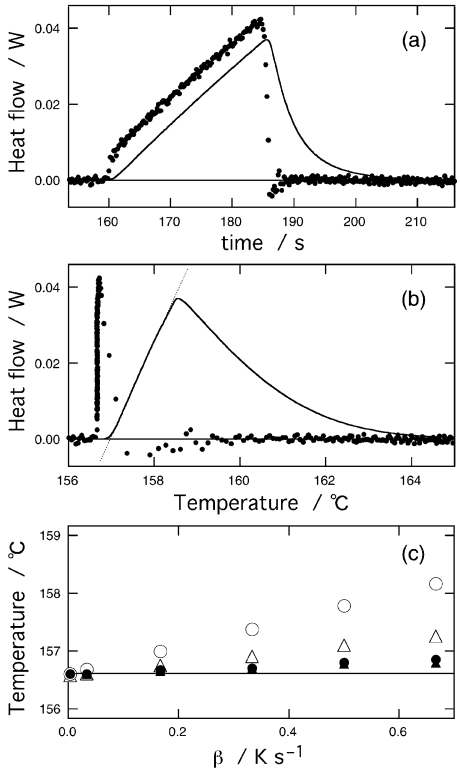

Fig. 7. The results of deconvolution of the instrumental effect in the melting of indium: plots of heat flow on transition, F (●), against time in (a) and against T_s in (b) for the heating rate of 10 K min^{-1} under nitrogen purge gas. Full lines in (a) and (b) represent the output heat flow signal of CDSC, plotted against time in (a) and T_m in (b); the heat flow is determined from the difference of temperatures of the monitoring stations at the sample and reference sides. In (c), the peak temperature of F, T_s^{peak}, (filled symbols) and the onset temperature of the output heat flow signal of CDSC, T_m^{onset}, (open symbols) are plotted against the heating rates of 0.2, 2.0, 10, 20, 30 and 40 K min^{-1} for nitrogen (○, ●) and helium (△, ▲) purge gases. Sampling interval was 0.2 s and sample weight was 22.84 mg.

$K_0 = 24$ mW K^{-1} and $K_1 = 96$ mW K^{-1} for helium purge gas and $C_m = 40$ mJ K^{-1}, $K_0 = 13.7$ mW K^{-1} and $K_1 = 24$ mW K^{-1} for nitrogen purge gas. The difference in the thermal conductivity of those purge gases appears as the difference in the coefficients, K_0 and K_1.

With the instrumental coefficients, it is now possible to deconvolute the instrumental effect by the above mentioned method. Fig. 7 shows the typical result of deconvolution. In Fig. 7b, it is clearly seen that the apparent shift in the melting peak due to the instrumental effect is successfully deconvoluted and the sharp peak at the melting point has been reconstructed. As seen in Fig. 7c, the deviation of the peak temperature from the true melting point (156.6 °C) was less than 0.2 K even for the fastest heating rate of 40 K min^{-1} irrespective of the choice of purge gas; the deviation will be caused by the thermal contact between indium and aluminum sample pan. It is also noted that the tail of the peak in F seen in Fig. 7b will also be due to the thermal contact and long interval of sampling time (0.2 s), as can be seen in the numerical calculation in Fig. 2c.

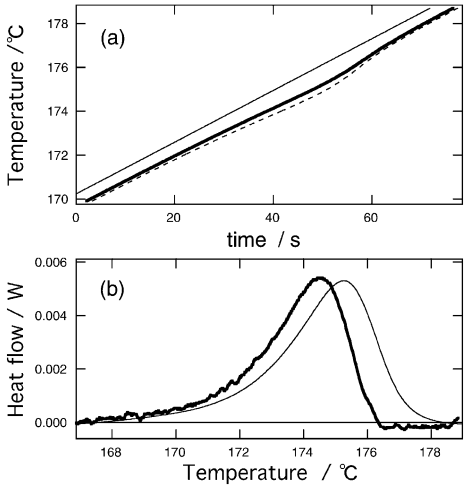

Fig. 8. A typical example of deconvolution of instrumental effect from the data of T_m in the melting region of iPP crystals at the heating rate of 7.0 K min^{-1}. In (a), T_h (thin line) and T_s (broken line) were calculated from T_m (thick line) with Eqs. (2), (3) and (5). In the calculation, the heat capacity of $C_s = 25.2$ mJ K^{-1} was utilized from TMDSC analysis with a standard method. In (b), the deconvoluted heat flow, F, (thick line) on melting is reconstructed from T_m, T_h, and T_s with Eq. (1) and plotted against T_s. The thin line in (b) represents the output heat flow signal of CDSC plotted against T_m.

4.2. Melting of iPP

Fig. 8 shows typical experimental data in the melting region of iPP crystals well annealed near the melting region beforehand. The deconvolution of the instrumental effect has been done to the data of temperature at the monitoring station, T_m, following Eqs. (1)–(3). In the deconvolution, we neglected the temperature dependence of the instrumental coefficients and utilized the values determined with the melting of indium at the melting point (156.6 °C); the temperature dependence is known to be small [14] and the changes in the values do not introduce significant error in the deconvolution.

Fig. 9 shows the heating rate dependence of melting peak temperature of iPP crystals. Fig. 9a shows the comparison of the calibration results of the present deconvolution method and of the conventional method with the onset temperature of the melting of indium. It is clearly seen that the estimated degree of the apparent shift due to instrumental delay is actually different for those methods. The apparent shift due to the instrumental effect depends on the choice of purge gas giving different thermal contact between sample pan and monitoring station and on the sample mass determining the peak height of the endothermic heat flow. In Fig. 9c, it is clearly seen that the results of the present method of deconvolution are not influenced by those effects and confirm the applicability of this method.

In order to confirm the applicability, it is further required to examine the influence of thermal conductance in the sample, which produces temperature gradient and contributes to the shift in the peak temperature. To see the effect

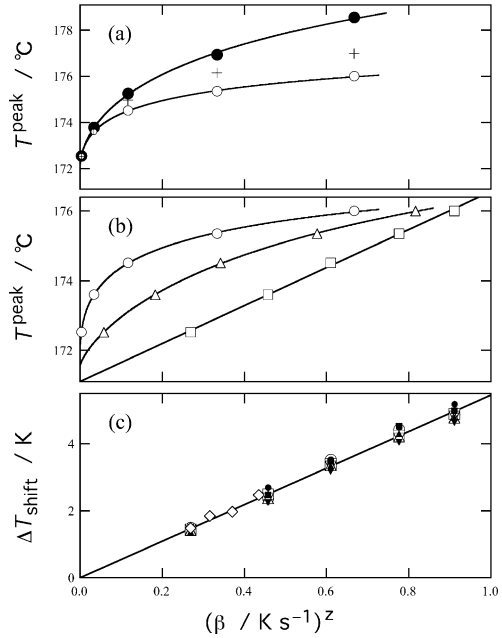

Fig. 9. Heating rate dependence of melting peak temperature of iPP crystals. In (a), the raw data of peak temperature, T_m^{peak}, (●) and the results of deconvolution, T_s^{peak}, (○) are plotted against β^1 for the sample of 2.22 mg in weight and 95 μm in thickness under nitrogen purge gas. The symbol + in (a) represents the calibration with the use of the heating rate dependence of the onset temperature of indium melting shown in Fig. 7. In (b), the results of deconvolution, T_s^{peak}, are plotted against β^1 (○), $\beta^{0.5}$ (△), and $\beta^{0.23}$ (□). In (c), ΔT_{shift} is determined from the linear fitting of T_s^{peak} vs. $\beta^{0.23}$ such as shown in (b), and plotted against $\beta^{0.23}$ for different sample mass/thickness and purge gases of helium (open symbols) and nitrogen (filled symbols): 0.36/17 (○, ●), 1.15/55 (△, ▲), 2.22/95 (□, ■), 3.35/152 mg μm^{-1} (▽, ▼). The symbol, ◇, in (c) represents ΔT_{shift} determined from τ_{TM} shown in Fig. 11 on the basis of Eq. (23) with the adjustable parameter of τ_c/τ_{TM} to fit the straight line in (c).

in polymeric films, a thin film of iPP (15 μm thick) or indium (15 μm thick) was placed on top of thicker PE film (~130 μm thick), in between two PE films (~60 μm thick), and beneath the film (~130 μm thick), which is molten in the melting region of iPP and indium crystals. Because of the low thermal conductivity in the molten PE film, the peak temperature of iPP and the onset temperature of indium at the positions above the PE film and in between two PE films were higher than the temperature when they were beneath the PE film, and the difference increased with faster heating rate, as shown in Fig. 10. However, the maximum difference of about 0.2 K with the fastest heating rate of 40 K min^{-1} was not appreciably large compared with the total shift in peak temperature of iPP shown in Fig. 9b, and hence it is concluded that the effect can be neglected with film thickness less than 100 μm for the heating rate slower than 40 K min^{-1}. It also needs to be mentioned that, depending on the thermal contact between the top surface of the films and the cap of aluminum pan, the difference can be larger for the place on top of thicker PE film than the place in between two PE films and vice versa, as shown in Fig. 10a and b. It is further noted that the thermal contact between the surfaces

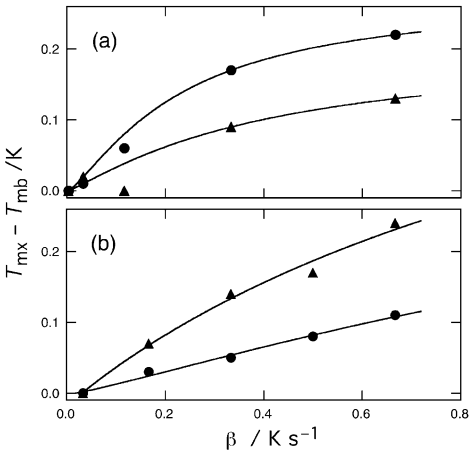

Fig. 10. The differences in (a) melting peak temperatures of iPP crystals and (b) the onset temperatures of melting in indium plotted against heating rate to see the effect of thermal conductance in a polymeric film. Melting of iPP or indium was examined with a film of 15 μm thick placed on top of thicker PE film of 130 μm (T_{mt}), in between two PE films of 60 μm (T_{mm}), and beneath the film of 130 μm (T_{mb}). The differences, $T_{mt} - T_{mb}$ (●) and $T_{mm} - T_{mb}$ (▲), are plotted for nitrogen purge gases.

of the films and aluminum pan can also be the source for necessary calibration. Applying silicone grease (Archer, 276–1372) between them resulted in the decrease in peak temperatures less than 0.1 K, so that we have concluded that the effect will be negligible for the examined heating rates.

After those considerations, the results of deconvolution shown in Fig. 9a still shows a remarkable shift in peak temperatures, which should be attributed to superheating effect. As shown in Fig. 9b, it is apparent that the heating rate dependence cannot be fitted with $z = 1$ ($R \propto \Delta T^0$) or $z = 0.5$ ($R \propto \Delta T^1$) but with $z = 0.23$ ($R \propto \Delta T^{3.3}$), and hence the dependence of R on ΔT must be non-linear. The

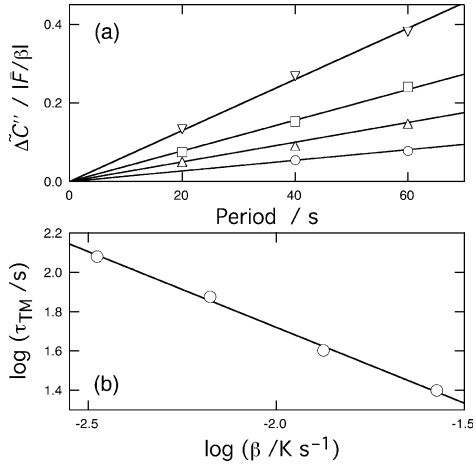

Fig. 11. (a) The dependence on modulation period ($\propto \omega^{-1}$) of the imaginary part of the apparent heat capacity obtained by TMDSC at the peak temperature in the melting region of iPP under helium purge gas at the underlying heating rate of 0.2 (○), 0.4 (△), 0.8 (□), and 1.6 K min^{-1} (▽). (b) Logarithmic plots against underlying heating rate of the characteristic time, τ_{TM}, chosen for the fitting shown in (a) with Eq. (28). Sample was of 2.22 mg in weight and 95 μm in thickness.

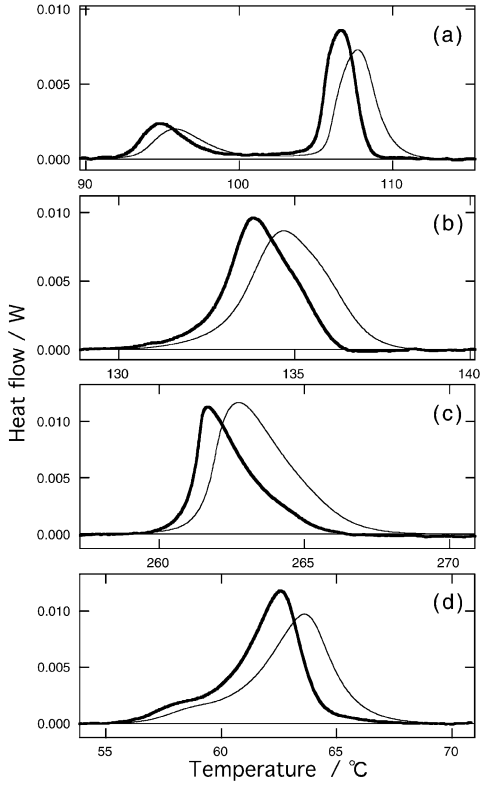

Fig. 12. Typical examples of deconvolution of instrumental effect from the data of T_m in the melting region of (a) LDPE, (b) PE, (c) PET and (d) PCL crystals: deconvoluted heat flow, F, plotted against T_s (thick lines) and the output heat flow signal of CDSC plotted against T_m (thin lines). The purge gas was nitrogen. The sample mass/thickness and the heating rate are the followings: (a) 2.3/97 and 10, (b) 1.1/44 and 7.0, (c) 4.0/100 and 10, (d) 2.3/100 mg μm^{-1} and 10 K min^{-1}.

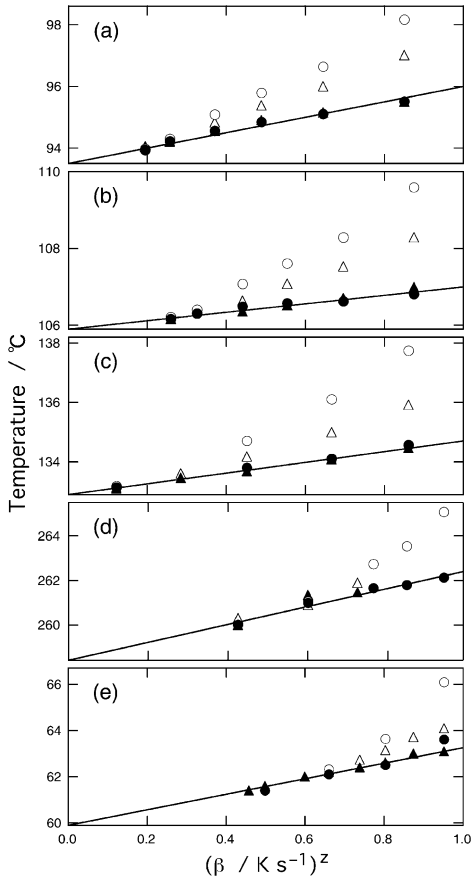

Fig. 13. Heating rate dependence of melting peak of (a) LDPE (lower peak), (b) LDPE (higher peak), (c) PE, (d) PET and (e) PCL plotted against $\beta^{0.40}$, $\beta^{0.33}$, $\beta^{0.37}$, $\beta^{0.15}$, and $\beta^{0.12}$, respectively. The symbols represent the raw data of peak temperature, T_m^{peak}, (open symbols) and the results of deconvolution, T_s^{peak}, (filled symbols) for the data with nitrogen (○, ●) and helium (△, ▲) purge gases. The sample thickness was 100 μm for LDPE, PET and PET, and 44 μm for PE.

degree of superheating, ΔT_{shift}, in Fig. 9c gives the characteristic time of $\tau_c = 6.1\beta^{-0.77}$ from Eqs. (19) and (23). On the other hand, Fig. 11 shows the results of TMDSC analysis giving the characteristic time of $\tau_{TM} = 1.5\beta^{-0.77}$. Therefore, the agreement of the β dependence expected from Eqs. (19) and (27) is confirmed satisfactorily. The ratio of the characteristic times, $\tau_c/\tau_{TM} = 4.0$, follows the predicted value of $\tau_c/\tau_{TM} = 4.3$ calculated from Eq. (26) with $y = 3.3$.

4.3. Melting of LDPE, PE, PET and PCL

Fig. 12 shows typical experimental data and the deconvolution results in the melting region of LDPE, PE, PET and PCL. Fig. 13 shows the heating rate dependence of the melting peak temperatures in those polymers. In Fig. 13, it is clearly seen that the raw data with nitrogen purge gas shows stronger dependences on heating rate than those of He purge gas because of lower thermal conductivity. After the deconvolution of the instrumental effect, we can confirm the agreement of the results with different purge gases of nitrogen and helium. The agreement of the power, z, for the results of CDSC (ΔT_{shift}, Eq. (23)) and TMDSC (β τ_{TM},

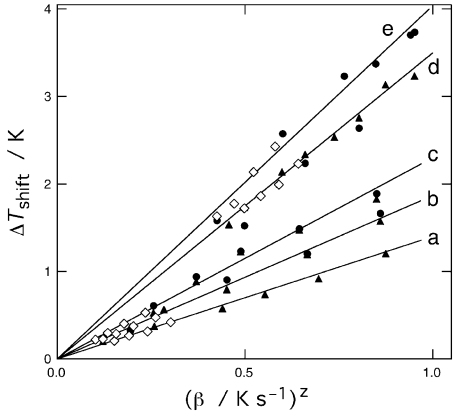

Fig. 14. Plots of ΔT_{shift} determined from the linear fitting of T_s^{peak} vs. β^z shown in Fig. 13. The symbols represent ΔT_{shift} for (a) LDPE (lower peak, $z = 0.40$), (b) LDPE (higher peak, $z = 0.33$), (c) PE ($z = 0.37$), (d) PET ($z = 0.15$) and (e) PCL ($z = 0.12$) under nitrogen (●) and helium (▲) purge gases. The symbol, ◇, represents ΔT_{shift} determined from τ_{TM} on the basis of Eq. (23) with the adjustable parameter of τ_c/τ_{TM} to fit the respective lines.

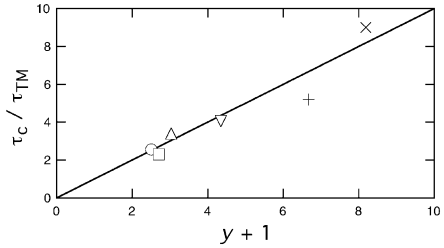

Fig. 15. The ratio, τ_c/τ_{TM}, for LDPE, PE, iPP, PET and PCL determined from the fitting of τ_{TM} shown in Figs. 9b and 14: LDPE (lower peak, ○), LDPE (higher peak, △), PE (□), iPP (▽), PET (+), and PCL (×). The full line represents the relationship of Eq. (26).

Eq. (27)) is also confirmed by the linear fitting of the plots shown in Fig. 14. Fig. 15 shows the ratio, τ_c/τ_{TM}, for those polymers determined from the fitting; the relationship follows the prediction of Eq. (26) satisfactorily for the power, $y \sim 1.5$–7.3 ($z \sim 0.12$–0.4), of those polymers.

5. Discussions

In the present paper, based on the modeling of superheating effect of melting kinetics, heating rate dependence of melting of polymer crystals has been examined experimentally for iPP, LDPE, PE, PET and PCL, which showed a variation of ΔT dependence of melting rate and suited for the purpose to examine the broad applicability of the present approach.

In the analysis, we have firstly examined the apparent shift in the melting peak temperature due to instrumental thermal delay on the basis of the Mraw's model of CDSC-HF and determined the instrumental coefficients required for the calibration by using the melting of indium. In comparison to the calibration results for the onset temperature in the melting of indium and the peak temperature in the melting of polymer crystals shown in Figs. 7c and 13, respectively, it is clearly seen that the estimated degree of the apparent shift due to instrumental delay is actually different for the onset temperature and the peak temperature because of the dependence on the peak height and its slope, which is automatically taken into account in the method. The empirical method of using the onset temperature of standard material is therefore not justified for the calibration of the peak temperature in the melting of polymer crystals.

The present method of deconvolution of instrumental effect utilizes only the data of temperature at the monitoring station of the sample side. If we make use of the difference of temperatures at the sample and reference sides, as has been done in CDSC-HF, a small time lag between those data, which are amplified from the original signals by way of different electric circuits, is unavoidable; hence the deconvolution needs fine tuning of those data with smaller interval of sampling time. On this point, refinement of the instrument may be worth trying. On the other hand, only with the data of sample side, signal to noise ratio of the transition peak becomes worse with slower heating rate, and hence the heating rate is limited to $\beta > 1$ K min^{-1} for the practical purpose of deconvolution in the melting region of polymer crystals. However, with slower heating rate, the instrumental effect can be negligible, as seen in Figs. 9a and 13, and hence the disadvantage does not cause serious difficulty in this method.

It is further noted that the temperature control of the heat source in CDSC-HF is not influenced by the feedback of sample temperature, and hence the deconvolution process with Eqs. (1)–(3) is straightforward. On the other hand, with a DSC of power compensation type, the procedure is quite complicated [31] because DSC of power compensation type adjusts the output of a heater placed close to the sample to control the temperature at the monitoring station under the influence of the feedback of sample temperature especially on transition. The present method of deconvolution will also be more favorable than the method utilizing the information about the slope and height of a peak [26] because we are free from any assumption about the transition kinetics with the present method.

Utilizing the instrumental coefficients determined by the melting of indium, we have examined the melting behavior of iPP with different purge gases and sample mass and confirmed that the apparent shift in peak temperature due to instrumental delay can be successfully eliminated. The effect of thermal conductivity in the sample has also been examined with iPP + PE and In + PE, and we have concluded that this effect introduces the difference of only 0.2 K even with the fastest heating rate of $\beta = 40$ K min^{-1} for thin samples with thickness less than 100 μm. After excluding those apparent shifts, heating rate dependence of the shift in peak temperature of iPP has been fitted with the power of $z = 0.23$. The dependence indicates that the power of τ_c is $x = 0.77$ from Eq. (23), and the power is consistent with the power of τ_{TM} determined by TMDSC in terms of the relationship expressed by Eqs. (19) and (27). For other polymers of LDPE, PE, PET and PCL, the relationship has also been confirmed successfully. Concerned with the absolute values of τ_c and τ_{TM}, the experimental results with iPP, LDPE, PE, PET and PCL follow the prediction of Eq. (26), as shown in Fig. 15.

This type of approach to the ΔT dependence of melting rate utilizing the heating rate dependence of peak temperature was originally recognized by Schawe and Strobl [24] and Sohn et al. [32]. The present results confirm the applicability of this approach after eliminating the apparent shift due to instrumental delay. The applicability of the analysis of TMDSC is also confirmed by the good agreement of the results of TMDSC and CDSC-HF, based on the relationship of Eq. (26).

Concerned with the ΔT dependence of the melting rate coefficient expressed as Eq. (17), the power of τ_c and τ_{TM} suggests that the melting rate of iPP crystals depends on ΔT with the power of $y = 3.3$. For LDPE and PCL, the power, y, ranges from 1.5 to 7.3. Therefore, the dependences of

different polymers showed a variety in the range from nearly linear dependence to much stronger dependence, which corresponds to an exponential dependence in the limiting case. Among them, linear dependence can be explained by the following two cases; one is interfacially controlled growth without nucleation barrier and another is limited by heat diffusion with the interfacial temperature kept at the transition point due to the endothermic process of melting. Slower process between them controls the kinetics. In both cases, melting rate is in proportion to the difference between the melting point and the mean sample temperature, namely the degree of superheating, ΔT. The differentiation of those processes is difficult, but may be possible if we carefully consider the difference in the time development of linear growth in the former case and $t^{1/2}$ behavior in the latter. The examination of the details of the melting kinetics needs morphological information especially on the growth interface, which will certainly require further investigation with microscopy.

Non-linear dependence on ΔT of the melting rate coefficient indicates an activation process such as nucleation. Melting kinetics is usually supposed to be free from activation barrier because crystals can start melting from the corners without nucleation. However, because of the following reason, melting of polymer crystals can be an exceptional case. Firstly, we have to recognize that polymer crystals are not in the most stable state, in which chains must be extended. With chain folding, the melting point is therefore determined by the balance between the bulk free energy difference of crystalline and molten states and the excess surface free energy mainly attributed to the excess energy of chain folding. The relationship known as Gibbs–Thomson effect [1] is expressed as

$$\ell \frac{\Delta h_f}{T_M^0}\left(T_M^0 - T_M\right) = 2\sigma_e \tag{29}$$

where ℓ represents the lamellar thickness, Δh_f represents the heat of fusion per unit volume, and T_M^0 is the equilibrium melting point of an extended chain crystal. With the excess surface free energy, σ_e, the non-equilibrium melting point, T_M, can be much lower than the equilibrium melting point.

Secondly, for the crystals grown from the melt, we know that the chains are not always folded back to the adjacent stem because the interpenetrated random coils in the molten state are only weakly perturbed by the crystallization process [33]. Therefore, we expect a large fraction of long loops of chains connecting non-adjacent stems in the same lamella or neighboring lamellar crystals. For those stems, some stems are more stable than others, and the drop of melting point expressed by Eq. (29) will be different for each stem with the variation in the excess free energy, σ_e, at both ends. It means that, even if melting can start from the corners of a crystal without nucleation, the melting interface cannot be always propagated through those stems with a distribution of melting points in a single lamellar crystal. On the other hand, it is probable to initiate melting sporadically at those stems with lower melting points in the interior of the lamellar crystal. The process will create melting interface surrounding the stems, so that it needs to be thermally activated as a nucleation process.

Assuming nucleation-controlled transition with a two-dimensional nucleus, valuable information about the kinetics can be obtained from the melting rate coefficient in the following way. Firstly, for the transition kinetics controlled by primary nucleation, the rate coefficient of a cylindrical nucleus with the interfacial free energy at the side surface, σ, will be expressed as [34],

$$R = R_0(T_s)\exp\left(-\frac{K}{\Delta T_n}\right) \tag{30}$$

$$K \equiv \frac{\pi \ell \sigma^2 T_M^0}{k_B \Delta h_f T_s} \tag{31}$$

$$\Delta T_n \equiv T_s - T_M \tag{32}$$

where R_0 represents a pre-exponential factor weakly dependent on temperature and k_B is the Boltzmann constant. If we can neglect the change in the absolute temperature, T_s, compared with the change in ΔT_n, the coefficient, K, is supposed to be constant.

The dependence of R on ΔT_n can be approximately expressed as an exponential dependence. For the exponential dependence, the characteristic time, τ_{TM}, is expressed as [10,11],

$$\log R \propto c\Delta T_n \tag{33}$$

$$\tau_{TM} = (c\beta)^{-1} \tag{34}$$

With the following relationship, the coefficient, K, of Eq. (31) can be determined from the coefficient, c, in τ_{TM} of Eq. (27) experimentally,

$$c = \frac{\mathrm{d}(\log R)}{\mathrm{d}T} \cong \frac{K}{\Delta T_n^2} \tag{35}$$

If we compare the expression of Eqs. (27) and (34), it is apparent that the application of this procedure requires the confirmation of the power of $x = 1$ which corresponds to the limiting case of $y \to \infty$ for the ΔT dependence of R in Eq. (17). For PCL and PET, the power, x, is close to 1, and hence the application will be justified. For iPP, PE and LDPE with $x < 1$, the coefficient, K, is overestimated, but the rough estimate of the coefficient will be made by this analysis.

In the expression of K, we can estimate the unknown parameters of the product of surface free energy and lamellar thickness, $\sigma^2\ell$ with the known values of T_M^0 and Δh_f [35–37]. Fig. 16 shows the results of this analysis at the peak temperature, $T_s = T_s^{peak}(\beta)$, with $T_M = T_s^{peak}(0)$ in Eq. (32); the interfacial free energy in Fig. 16c is scaled by the heat of fusion, Δh_f, and intermolecular spacing in the crystal, d. The change in this value is consistent with the change in the power, x, in the sense that larger value

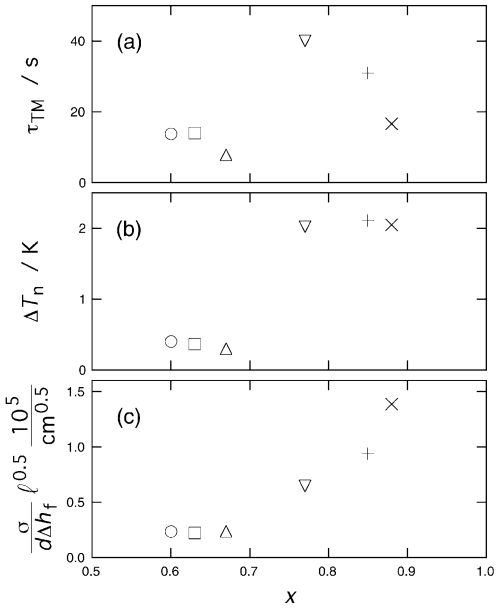

Fig. 16. (a) τ_{TM} determined by TMDSC at the underlying heating of 0.8 K min^{-1} under helium purge gas. (b) ΔT_n determined from the results of CDSC-HF shown in Figs. 9b and 14 for $\beta = 0.8$ K min^{-1}. (c) $(\sigma/d\Delta h_f)\ell^{0.5}$, determined from τ_{TM} and ΔT_n with Eqs. (31), (34) and (35). The values are plotted aainst the power x. The symbols represent the results for LDPE (lower peak, ○), LDPE (higher peak, △), PE (□), iPP (▽), PET (+), and PCL (×).

corresponds to larger x (and y) indicating stronger dependence on ΔT_n of melting rate with higher activation of nucleation. It is empirically known from Thomas–Staveley relationship [38] that the ratio, $\sigma/(d\Delta h_f)$, is about 0.1–0.15 for the crystal nucleation from the melt of polymers [39,40]. If we assume a typical lamellar thickness of $\ell = 10$ nm, the ratio calculated from the results for PCL, PET and iPP is about 0.01, and becomes much smaller for PE and LDPE; because we take the square root of ℓ in Fig. 16c, the results are not strongly influenced by the choice of the value of ℓ. The smaller value of this ratio may indicate the roughening of the crystal-melt interface in the temperature range of melting. It is also noted that weaker dependence with less activation barrier for polyethylene and iPP seems to be related with the high mobility of polymer chains in the crystalline state, which is characterized by the existence of crystal dispersion observed by various relaxation phenomena [41]. The high mobility will promote a large-scale reorganization of chains to have a homogenization of melting points of stems, which may make it possible to complete the melting from the corners of crystals without nucleation process. Further studies will be certainly required to clarify the mechanism of the melting process with other means of experimental examinations.

In the final part of discussion, it will be worth mentioning about the merits and demerits of those two methods of examining heating rate dependence with CDSC-HF (τ_c) and frequency dependence with TMDSC (τ_{TM}). (1) Concerned with the information about the kinetics at the peak temperature, both methods can provide essentially identical information, as we have confirmed in the above. However, TMDSC will be better in its ability to analyze the kinetics in the whole transition range to see the frequency dependence at the respective temperatures. In order to do the same analysis with CDSC-HF, the deconvolution of the distribution of melting points, $\phi_0(T_M)$, in Eq. (21) will not be straightforward; with TMDSC the deconvolution is related with the condition of (quasi-)steady state and can be inessential for the modulation period short enough compared with the width of melting peak. (2) Periodic modulation in driving force with TMDSC has an essential limitation in the range of applicable heating rate because the response must be in a (quasi-)steady state for the Fourier analysis. It means that the period of modulation must be short enough compared with the residence time in the transition region with underlying heating; this condition cannot be satisfied with faster heating rate. (3) If recrystallization and/or reorganization are active, heating rate applicable with CDSC-HF is limited only to fast heating in order to avoid those processes. With TMDSC, it is known that those processes are not sensitive to temperature modulation [10–15], and hence we can apply slower underlying heating rate. (4) For stronger dependence of R on ΔT with increasing y, it is more difficult to determine the power, z, from the fitting such as shown in Figs. 9a and 13 by CDSC-HF, because z approaches to zero with increasing y. On the other hand, with TMDSC the power, x, of τ_{TM} increases with y, and hence the determination is easier than that of CDSC-HF. (5) For the application of the present calibration in CDSC-HF, the stability of the baseline of the temperature at the monitoring station is essential, and hence the calibration of much broader heat flow peak (≥30 K) will not be practical. With TMDSC, the stability is not essential because TMDSC uses the modulation components in temperatures. (6) In order to apply the analysis to evaluate the interfacial free energy, we need to know the transition point, $T_s^{peak}(0)$, which is available only with CDSC-HF from Eq. (23) by the fitting such as shown in Figs. 9a and 13. In this sense, TMDSC cannot be independent of the application of CDSC-HF. After those considerations, it will be concluded that the combination of those methods will be most favorable. It should also be noted that the determination of $T_s^{peak}(0)$ in Eq. (23) with the fitting in Figs. 9a and 13 will be essential in the application of Gibbs–Thomson relationship expressed in Eq. (29) and of Hoffman–Weeks [42] plot of T_s^{peak} vs. crystallization temperature to determine the true melting point, T_M^0, by extrapolation. If the heating rate dependent $T_s^{peak}(\beta)$ is utilized in the analysis, the resultant T_M^0 will be inevitably influenced by the effect of superheating in the melting kinetics, and hence will be overestimated.

6. Conclusions

We have modeled the transition kinetics of melting in

polymer crystallites with a rate coefficient in proportion to the yth power of ΔT and introduced two characteristic times of τ_c and τ_{TM} to characterize the melting kinetics at the peak temperature in terms of the degree of superheating obtained with CDSC and the frequency dependence of the apparent heat capacity obtained with TMDSC, respectively. From the heating rate dependence of those characteristic times, the dependence on ΔT of the melting rate coefficient has been determined. The superheating dependence represented by the power, y, showed nearly linear dependence for LDPE ($y = 1.5$ and 2.0) and PE ($y = 1.7$) and non-linear dependence for iPP ($y = 3.3$), PET ($y = 5.7$) and PCL ($y = 7.3$). The linear dependence indicates the kinetics controlled by heat diffusion or by surface kinetics on rough interface. The non-linear dependence approaches to the limiting case of exponential dependence expected for nucleation-controlled kinetics of melting. We have proposed a possible nucleation mechanism of melting in polymer crystallites, in which the stability of each crystalline stem is expected to vary because of the variation of chain folding with large fraction of non-adjacent reentry.

Concerned with the nucleation mechanism, the interfacial free energy with a cylindrical nucleus has been evaluated from τ_{TM}. The change in the obtained values is consistent with the change in the power, y; namely the interfacial free energy is lower for the polymers of smaller power, y, which indicates less activation of nucleation barrier. The obtained value scaled by the heat of fusion, $\sigma/(d\Delta h_f)$, is much smaller than expected with Thomas–Staveley relationship and indicates the roughening of the interface. The behaviors will be related with the nature of polymer molecules in the crystalline state near the melting point and will need further investigation by other experimental means.

For the detailed analysis with CDSC-HF, we have applied a calibration method which is essentially the same as the one Danley and Caulfield [27] originally proposed. The method utilizes the deconvolution of instrumental effect on the basis of the Mraw's model with the instrumental coefficients pre-determined by the melting of indium.

Acknowledgements

The authors thank Mr K. Sasaki (TOYOBO Co. Ltd.) for the kind supply of poly(ethylene terephthalate). The authors are grateful to Dr Alizadeh and Prof. Marand (Virginia Polytechnic Institute and State University) for their valuable discussions. The authors also acknowledge valuable discussions with Prof. Schick (University of Rostock) on the influence of thermal contact between sample and pan. This work was partly supported by a Grant-in-Aid for Scientific Research from Japan Society for the Promotion of Science.

References

[1] Wunderlich B. Macromolecular physics, vol. 3. New York: Academic Press, 1980.
[2] Hellmuth E, Wunderlich B. J Appl Phys 1965;36:3039.
[3] Hellmuth E, Wunderlich B, Rankin Jr. JM. Appl Polym Symp 1966;2:101.
[4] Liberti FN, Wunderlich B. J Polym Sci, A-2 1968;6:833.
[5] Toda A, Oda T, Hikosaka M, Saruyama Y. Polymer 1997;38:231.
[6] Toda A, Oda T, Hikosaka M, Saruyama Y. Thermochim Acta 1997;293:47.
[7] Toda A, Tomita C, Hikosaka M, Saruyama Y. Polymer 1997;38:2849.
[8] Toda A, Tomita C, Hikosaka M, Saruyama Y. Polymer 1998;39:1439.
[9] Toda A, Arita T, Tomita C, Hikosaka M. Polym J 1999;31:790.
[10] Toda A, Tomita C, Hikosaka M, Saruyama Y. Polymer 1998;39:5093.
[11] Toda A, Tomita C, Hikosaka M, Saruyama Y. Thermochim Acta 1998;324:95.
[12] Toda A, Tomita C, Hikosaka M. J Therm Anal 1998;51:623.
[13] Toda A, Arita T, Tomita C, Hikosaka M. Thermochim Acta 1999;330:75.
[14] Toda A, Arita T, Tomita C, Hikosaka M. Polymer 2000;41:8941.
[15] Toda A, Arita T, Hikosaka M. J Mater Sci 2000;35:5085.
[16] Toda A, Takahashi Y, Arita T, Hikosaka M, Furukawa T. J Chem Phys 2001;114:6896.
[17] Toda A, Arita T, Hikosaka M. J Therm Anal Calor 2000;60:821.
[18] Gill PS, Sauerbrunn SR, Reading M. J Therm Anal 1993;40:931.
[19] Reading M, Elliott D, Hill VL. J Therm Anal 1993;40:949.
[20] Reading M, Luget A, Wilson R. Thermochim Acta 1994;238:295.
[21] Wunderlich B, Jin Y, Boller A. Thermochim Acta 1994;238:277.
[22] Boller A, Jin Y, Wunderlich B. J Therm Anal 1994;42:307.
[23] Hatta I. Jpn J Appl Phys 1994;33:L686.
[24] Schawe JEK, Strobl GR. Polymer 1998;39:3745.
[25] Wunderlich B. In: Turi A, editor. Thermal characterization of polymeric materials. San Diego: Academic Press, 1997. Chapter 2.
[26] Schawe JEK. Thermochim Acta 1993;229:69.
[27] Danley RL Jr, Caulfield PA. Proceedings of the 29th NATAS Conference 2001:673.
[28] Mraw SC. Rev Sci Instrum 1982;53:228.
[29] Saito Y, Saito K, Atake T. Thermochim Acta 1986;99:299.
[30] Hatta I, Muramatsu S. Jpn J Appl Phys 1996;35:L858.
[31] Zucca N, Erriu G, Onnis S, Zedda D, Longoni A. Thermochim Acta 2001;366:15.
[32] Sohn S, Alizadeh A, Marand H. Polymer 2000;41:8879.
[33] Sperling LH. Physical polymer science. New York: Wiley, 1986. p. 195.
[34] Cormia RL, Price FP, Turnbull D. J Chem Phys 1962;6:1333.
[35] Tadokoro H. Structure of crystalline polymers. New York: Wiley, 1979.
[36] Wunderlich B. Pure Appl Chem 1995;67:1019 http://web.utk.edu/~athas/databank/intro.html
[37] Magill JH. In: Brandrup J, Immergut EH, Grulke EA, editors. Polymer handbook. New York: Wiley, 1999. Chapter VI.
[38] Thomas DG, Staveley TA. J Chem Soc 1952;1952:4569.
[39] Hoffman JD, Davis GT, Lauritzen Jr. JI. In: Hannay NB, editor. Treatise on solid state chemistry, vol. 3. New York: Plenum Press, 1976. Chapter 7.
[40] Turnbull D, Spaepen F. J Polym Sci, Polym Symp 1978;63:237.
[41] McCrum NG, Read BE, Williams G. Anelastic and dielectric effects in polymeric solids. London: Wiley, 1967.
[42] Hoffman JD, Weeks JJ. J Res Natl Bur Std 1962;66A:13.